CrystEngComm

Accepted Manuscript

ROYAL SOCIETY OF CHEMISTRY

www.rsc.org/crystengcomm

CrystEngComm

COMMUNICATION

Star-shaped VO_2 (M) Nanoparticles Film with High Thermochromic Performance†

Li Zhong,[ab] Ming Li,[a] Hua Wang,[ab] Yuanyuan Luo,[a] Jing Pan,[a] Guanghai Li*[ab]

Received 00th January 20xx,
Accepted 00th January 20xx

DOI: 10.1039/x0xx00000x

www.rsc.org/

Star-shaped VO_2 (M) nanoparticles were synthesized by hydrothermal reaction using only ammonium metavanadate and formic acid combined with subsequently mild annealing treatment. An enhanced thermochromic performance was demonstrated upon changing temperature and the applied pulse voltage for the star-shaped VO_2 (M) nanoparticles thin films.

Vanadium dioxide (VO_2) has a number of polymorphs. VO_2 (R) and VO_2 (M) with a rutile and monoclinically distorted rutile structure, respectively, posses a reversible metal-semiconductor transition.[1] Monoclinic VO_2 (B),[2] tetragonal VO_2 (A),[3,4] layer-structured VO_2 (C),[5] and recently reported VO_2 (D),[6] are metastable phase of VO_2. The metal-semiconductor transition between VO_2 (M) and VO_2 (R) takes place at the critical temperature of about 68 °C, and the optical and electrical properties change dramatically during the phase transition, which make VO_2 (M) widely applicable in the fields like sensors,[7,8] optical or electrical switch,[9-11] memory devices,[12] and smart windows.[13] Being suffering from cracking after the repeated reversible phase transition for single crystalline or bulk material, the nanostructured VO_2 (M) is thus received much attention due to its cycling stability and advantages in enhancing the optical and electrical properties.

Different methods have been explored to prepare VO_2 (M) nanomaterials, such as magnetron-sputtering,[14] vapour transport approach,[15] hydrothermal method,[16,17] and sol-gel method.[18] Because of cost-effective, high-production and structure and morphology-controlling, the hydrothermal method has been widely used to prepare VO_2 (M) nanostructures. However, there are two difficulties in the hydrothermal synthesis of VO_2 (M) nanoparticles (NPs). Firstly, hydrothermal reactions in solution often yield metastable phase of VO_2 (B) or VO_2 (A), and post high temperature annealing treatment is needed to transform these metastable phases to VO_2 (M), but annealing treatment at high temperatures always gives rise to a larger VO_2 (M) grain size.[19] And secondly, there are few reports on the one-step hydrothermal reaction to synthesize VO_2 (M) except at relative higher temperatures, which will also result in overgrowth of VO_2 (M) particles. In general, The VO_2 (M) obtained by hydrothermal synthesis is mesocrystalline snowflake or star-shaped particles.[20-24] How to prepare nanoscale VO_2 (M) by simple hydrothermal method is still a great challenge.

Hydrothermal synthesis of VO_2 (D) NPs is of benefit to acquire VO_2 (M) NPs.[6,25,26] Recently, VO_2 (M) NPs were successfully synthesized by hydrothermal method and annealing treatment of VO_2 (D) NPs.[27] Because substantial surfactants were used in the hydrothermal synthesis, subsequently superfluous wash is needed, and carbon contamination is inevitable after annealing treatment.

In this communication, we report the hydrothermal synthesis of star-shape VO_2 (D) NPs by using only ammonium metavanadate and formic acid without any surfactants. The VO_2 (D) NPs can be easily transformed to VO_2 (M) NPs by annealing at low temperatures. An enhanced thermochromic performance with high stability and reversibility of the VO_2 (M) NPs thin film was demonstrated.

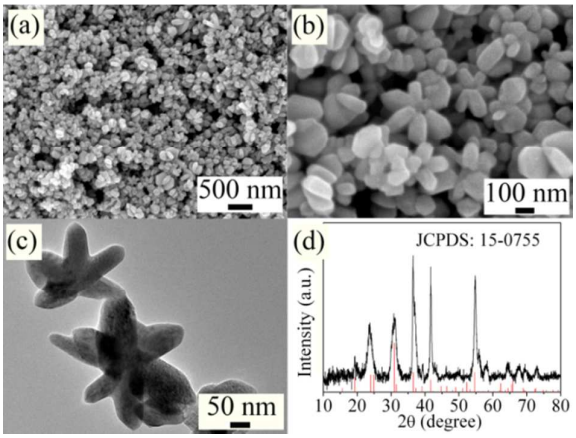

Fig. 1 (a) and (b) FESEM images, (c) TEM image and (d) XRD pattern of VO_2 (D) nanoparticles hydrothermal synthesis at 200 °C for two days.

[a] Key Laboratory of Materials Physics, Anhui Key Laboratory of Nanomaterials and Nanotechnology, Institute of Solid State Physics, Chinese Academy of Sciences, Hefei 230031, P. R. China. E-mail address: ghli@issp.ac.cn.
[b] School of Chemistry and Materials Science, University of Science and Technology of China, Hefei 230031, P.R. China.
[c] †Electronic Supplementary Information (ESI) available: [TEM and HRTEM images of a star-shaped VO_2 (D) NP composed of the intersected nanorods, FESEM image and the corresponding XRD pattern of the products synthesised at different conditions, cross section FESEM images of VO_2 (M) NPs thin films on glass substrate, Variable-temperature FT-IR spectra of the VO_2 (M) NPs thin film, optical photographs of Ag NWs transparent conducting film heater and VO_2 NPs/Ag NWs/glass device, the calculated integrated luminous and solar irradiation transmittance of VO_2 (M) NPs thin films]. See DOI: 10.1039/x0xx00000x

Figs. 1a and b show the FESEM images of the as-prepared powders. One can see that the powders are composed of short nanorods and hexagonal star-shaped particles with six arms, and the short nanorods or the arms have the length of about 100~130 nm and the thickness of about 60~80 nm. TEM observations proved that the star-shaped powders are hexagonal but with unsymmetrical character, as shown in Fig. 1c. All the XRD diffraction peaks shown in Fig. 1d can be well indexed to $NiWO_4$ (JCPDS card no.15-0755), indicating that the as prepared powders are metastable phase VO_2 (D) NPs, which is in accordance with Xie's report.[6] Detail FESEM observations and calculation indicate that the content of the star-shaped VO_2 (D) NPs is over 60 %.

The crystal structure and the orientation relationships in the star-shaped VO_2 (D) NPs were examined by TEM and HRTEM analysis, see Fig. S1. And the results indicates that the intersected interfaces of the star-shaped VO_2 (D) NPs are {112} planes, and the arms grow along ⟨110⟩ and ⟨112⟩ directions. In fact, a (020) twin in VO_2 (D) NPs was also accidentally observed, as shown in Fig. S2. This result indicates that there are other intersected interfaces.

The hexagonal star-shaped VO_2 (D) NPs have not been reported in the literatures. In our synthetic route, the formic acid is a key factor in synthesizing the star-shaped VO_2 (D) NPs because either pure VO_2 (B) NPs or nanorods are obtained if other reducer was used, such as oxalic acid,[27] or polyethylene glycol.[28] The star-shaped VO_2 (D) NPs can be obtained when the formic acid was in the range of about 1.5-4 ml, and once the star-shaped VO_2 (D) NPs shown in Fig. 1a were formed no further size and shape changes were observed with further increasing hydrothermal time. It was found that either VO_2 (B) NPs or the phase mixture of VO_2 (D) and VO_2 (B) was obtained with the formic acid lower than the content mentioned above. XRD analysis indicates that the phase of the star-shaped VO_2 (D) NPs is pure and no V_2O_3 or other impurities is present. These results indicate that the formic acid acting as modifier and reducer plays a critical role in the morphology and phase control of the star-shaped VO_2 (D) NPs in the hydrothermal process. If the hydrothermal temperature is at or lower than 180 °C VO_2 (B) nanorods were obtained, as shown in Fig. S3a and b. In fact, it has reported that the VO_2 (B) nanobelts can be synthesized under hydrothermal condition at 180 °C using the same reaction system as present study.[29] It was found that the size of the star-shaped VO_2 (D) NPs increases with increasing the hydrothermal temperature, as shown in Fig. S3c and d, which is a common phenomenon observed in the hydrothermal synthesis of nanomaterials. The hydrothermal time also play important roles in obtaining the star-shaped VO_2 (D) NPs in our reaction system. A shorter reaction time always leads to the formation of VO_2 (B) nanorods that is a common result mentioned in previous studies.

The star-shaped VO_2 (D) NPs is formed at the pH value of 1.5-2.5, and the VO_2 (B) phase will be formed if the pH value is higher than 2.5, and little products will be obtained if the pH value is lower than 1.5 because of excessive acidification. It was also found that addition of certain surfactant like Polyvinylpyrrolidone (PVP) and Cetyl Trimethyl Ammonium Bromide (CTAB) into the precursor solution will result in the formation of either star-shaped VO_2 (D) NPs with some overgrown particles (Figs. S4a and b) or the phase mixture of the star-shaped VO_2 (D) NPs and VO_2 (B) nanobelts (Figs. S4c and d). In the present work, VO_2 (D) NPs with star-shaped morphology were synthesized by hydrothermal reaction using only ammonium metavanadate and formic acid. The absence of other reactants and surfactants can not only make it easier to handle the reaction but also avoid any organic residues in the resulting product, which is different from our previous report.[27]

Above results demonstrate that the star-shaped VO_2 (D) NPs can be synthesized at temperature of 200 °C or higher, a pH value of 1.5-2.5 and a time of 48 hrs or longer under hydrothermal condition. The basic reaction can be formulated by following equation[29]:

$$2VO_3^- + HCOOH + 2H^+ \rightarrow 2VO_2 + CO_2 + H_2O \quad (1)$$

Firstly, V_2O_5 clusters will be created by stirring ammonium metavanadate in water, and under hydrothermal condition the VO_2 (B) crystal nuclei formed through the reduction reaction of formic acid will then transform to VO_2 (D) crystal nuclei, and finally the VO_2 (D) crystal nuclei will grow in size and form star-shaped VO_2 (D) NPs.

The monoclinic VO_2 (B) can be regarded as a layer structure in which the distorted [VO6] octahedra share both corner and edges,[30] while monoclinic VO_2 (D) is built up from octahedra at two slight distorted orientations, similar to VO_2 (R) phase.[6] Careful HRTEM analyses of the products at different hydrothermal growth stages at 200 °C shown that there are no orientation relationships between the VO_2 (B) and VO_2 (D) phases, and these two phases are always separate from each other. From this result we speculate that the phase transformation from VO_2 (B) to VO_2 (D) is a reconstructive one.

In the hydrothermal synthesis, the classic Ostwald ripening (OR) is a common crystal growth mechanism, in which the larger particles grow at the expense of smaller ones. The growth rate of larger particles is directly proportional to the solubility of solid and the tension of solid-liquid interfacial, and is affected by particle size distribution.[31] Oriented attachment (OA) is an another growth mechanism in which larger crystals form by crystallographically controlled assembly of smaller nanocrystals.[32] The exact formation mechanism of the star-shaped VO_2 (D) NPs is unknown right now. We speculate that the formation of the star-shaped VO_2 (D) NPs is essentially a facet-mediated aggregation and sequential elimination of high energy surfaces, owing to significant contribution of surface energy to the total free energy in a nanoscale system.

Figs. 2a and b show respectively the FESEM and TEM images of the star-shaped VO_2 (M) NPs after annealing VO_2 (D) NPs at 400 °C for 1 h. One can see that not only the morphology but also the size of

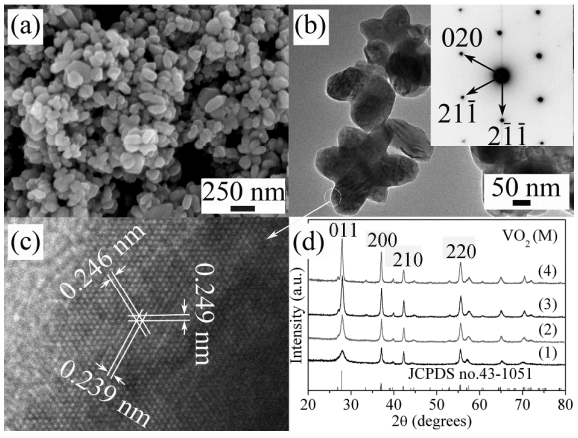

Fig. 2 (a) FESEM and (b) TEM images of VO_2 (M) NPs. The inset in (b) is the corresponding SAED pattern in the circle area([102] zone axis). (c) HRTEM images of the circle area in Fig. 2b. (d) XRD patterns of VO_2 (M) NPs annealed at temperature of (1)300, (2) 350, (3) 400 and (4) 450 °C.

the VO_2 (M) NPs nearly have no change after annealing treatment compared with that of the star-shaped VO_2 (D) NPs. The inset in Fig. 2b shows the corresponding SAED pattern of the end part of an arm of the star-shaped VO_2 (M) NPs, which proves that after annealing treatment, the VO_2 (D) phase has transformed to VO_2 (M) phase. The observed lattice spacing of 0.2389, 0.2458 and 0.2493 nm in Fig. 2c matches well respectively with the interplanar distance of (020), $(2\bar{1}\bar{1})$ and$(21\bar{1})$plane of VO_2 (M) (from [102] zone axis), which is compatible with corresponding report in literature,[33] and further proved the formation of VO_2 (M) phase. Fig. 2d shows the XRD patterns of VO_2 (M) NPs annealed at different temperatures, in which all the diffraction peaks can be indexed to monoclinic VO_2 (M) (JCPDS card no. 43-1051). From Fig. 2d one also can see that the higher the annealing temperature, the stronger the diffraction peaks, implying an improved crystallinity of the star-shaped VO_2 (M) at a higher annealing temperature. Further FESEM analyses indicate that the size of the star-shaped VO_2 (M) NPs only slightly increases with increasing annealing temperature form 300 °C to 450 °C.

The reversible structural phase transition of VO_2 (M) was investigated by DSC analysis. Fig. 3 shows the DSC curves of the star-shaped VO_2 (M) NPs annealed at temperature of 300, 350, 400 and 450 °C. One can see that, with increasing annealing temperature, the *Tc* increases from 50.51 to 68.62 °C during the heating cycle, and from 40.31 to 55.23 °C in the cooling cycle, while the thermal hysteresis width calculated from the DSC curves shows a monotonous increase from 10.2 to 13.59 °C. These results indicate that the lower the phase transition temperature, the narrower the hysteresis width, which is different from the results reported in literature,[34] in which the smaller NPs has a higher T_c and wider hysteresis due to the size effect. In the present study, the size of the star-shaped VO_2 (M) NPs only increases slightly, and thus the decrease in internal stress inside the VO_2 (M) NPs is considered the main reason of above phenomenon, as discussed in details in our recent work.[27] On the other hand the interfacial effect also plays an important role in narrowing the hysteresis width the star-shaped VO_2 (M) NPs, as the interfaces can act as a nucleation sites in the phase transition process. The existence of interfaces will reduce the driving force to trigger the phase transition of VO_2 (M) NPs, resulting in a lower T_c and a narrower hysteresis width.[27, 35]

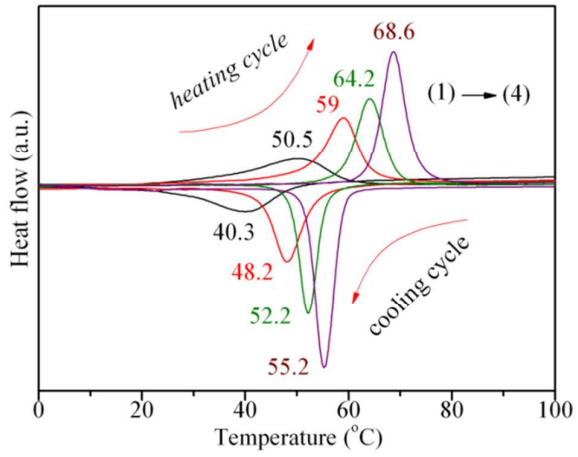

Fig. 3 DSC curves of VO_2 (M) nanoparticles annealed at temperature of (1) 300, (2) 350, (3) 400 and (4) 450 °C.

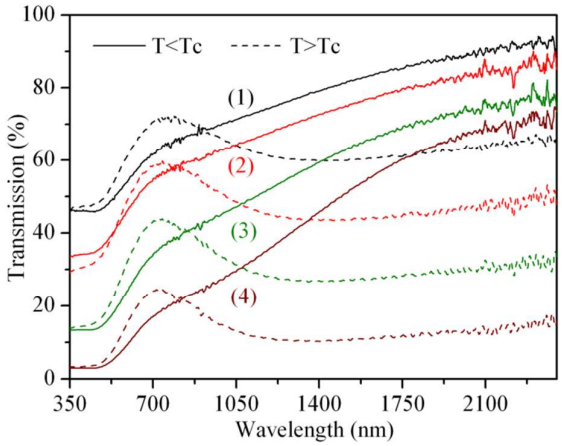

Fig. 4 Visible and infrared optical transmittance of VO_2 (M) NPs thin film on glass substrates before (25 °C, T<Tc) and after phase transition (100 °C, T>Tc) with the thickness of (1) 250, (2) 325, (3) 480 and (4) 510 nm.

To test the optical modulation ability, the VO_2 (M) NPs thin films were obtained by spin-coating VO_2 (M) dispersion solution with 2 wt% PVP and 2 wt% VO_2 (M) NPs in alcohol on glass substrate (the VO_2 (M) NPs are obtained by annealing VO_2 (D) NPs at 400 °C, the same for the VO_2 (M) NPs thin films mentioned below). The thickness of the film was controlled by changing the spin rate and the repeated time. Four thin films with the thicknesses of about 250, 325, 480 and 510 nm were prepared (the thickness of the thin films was estimated by the corresponding cross section FEMSEM image, as shown in Fig. S5). The optical transmittance of the four VO_2 (M) NPs thin films is shown in Fig. 4, and from which one can see that the thinner the film, the higher the optical transmittance in both visible and near-infrared regions, and the smaller the transmittance difference before and after phase transition.

The calculated integrated luminous and solar irradiation transmittance at both 25 °C and 100 °C decreases while the modulation ability of solar transmittance increases with increasing the film thicknesses except for the film with the thickness of 325 nm, which has a relative uniform luminous transmittance of 43-44 % and a solar transmittance modulation of over 7.32 %, see Table S1. This result indicates that the 325 nm VO_2 (M) NPs thin film has an optimal optical performance in both integrated luminous transmittance and modulation ability of solar transmittance.

From the variable-temperature FT-IR spectra of the VO_2 (M) NPs thin films with different thicknesses, we found that that the transmittance at wavenumbers of 4000-2000 cm^{-1} (2.5-5 μm) decreases monotonously with increasing temperature, and the infrared modulation amplitude is about 11, 13, 21 and 34 % at the wavenumbers of 3600-2500 cm^{-1} (2.78-4 μm) and about 19，25，34 and 57 % at wavenumbers of 4000-3700 cm^{-1} (2.5-2.7 μm) for the thin film with the thickness of 250, 325, 480 and 510 nm, respectively, as shown in Fig. S6. And here again the thicker film displays an enhanced optical regulation ability.

To study the stability and infrared regulation of the star-shaped VO_2 (M) NPS under external potential,[17] a device based on VO_2 (M) NPs thin film and Ag nanowires (NWs) transparent conducting electrode on glass substrate was constructed (the Ag NWs were synthesized by hydrothermal reaction,[36] and the Ag NWs transparent conducting electrode was made by doctor-blading the Ag NWs dispersion solution on glass substrate and then two parallel copper

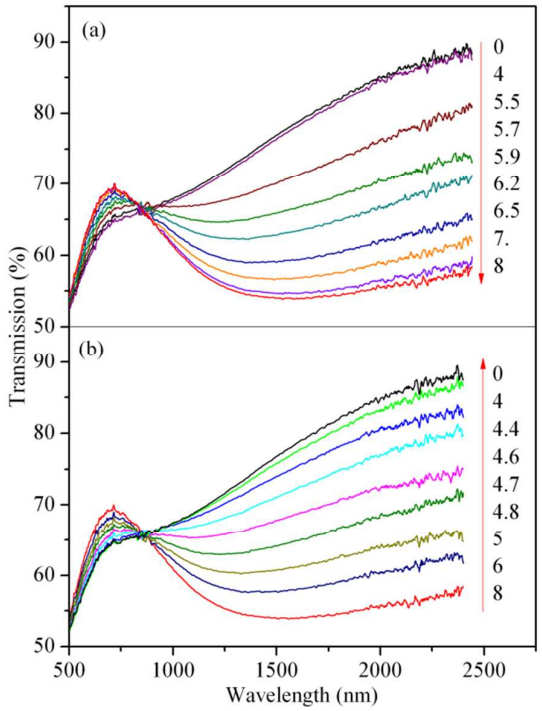

Fig. 5 Optical transmittance spectra of VO_2 NPs/Ag NWs/glass device with (a) increasing and (b) decreasing input voltage.

wires were pasted by Ag paste on the two side of the substrate as electrode), here the Ag nanowires (NWs) transparent conducting electrode was used as a film heater.[36,37] The VO_2 (M) NPs/Ag NWs/glass device is shown in Fig. S7. When an input voltage was applied to the electrodes, the heat will conduct from the Ag NWs film heater to VO_2 NPs thin film, and create a definite temperature environment on the device, and the higher the input voltage, the higher the temperature. Fig. 5 shows optical transmittance spectra of the device at different input voltages. One can see that the optical transmittance in the near infrared region gradually decreases with increasing the input voltage from 0 to 8 V, and completely recovery when gradually reduces the input voltage till 0 V. The variation of the infrared transmittance with input voltage has a similar tendency with temperature. This result demonstrate that a reversible phase transition can be triggered by an input voltage for the VO_2 NPs, indicating the infrared transmittance can be dynamically modulated by external potential. From Fig. 5 one also can see that the minimum input voltage that can induce a considerable change in infrared transmittance is lower than the spherical VO_2 (M) NPs reported in our previous study.[17] This result indicates that the infrared switching of the star-shaped VO_2 (M) NPS can be trigged at a relative low voltage, which is beneficial for practical applications.

Fig. 6a shows the infrared transmittance of the device at 1.5 μm upon a periodic square-wave with different amplitudes (the cycle of the square-wave pulses is 2 min). One can see that the transmittance gradually drops to a equilibrium value when a constant voltage is applied and recovers its original value once the input voltage is removed, and the higher the pulse amplitude, the higher the infrared transmittance drop, and thus the higher the infrared modulation. The equilibrium value of the infrared transmittance upon an applied pulse voltage depends on the duration time of the pulse, the longer the

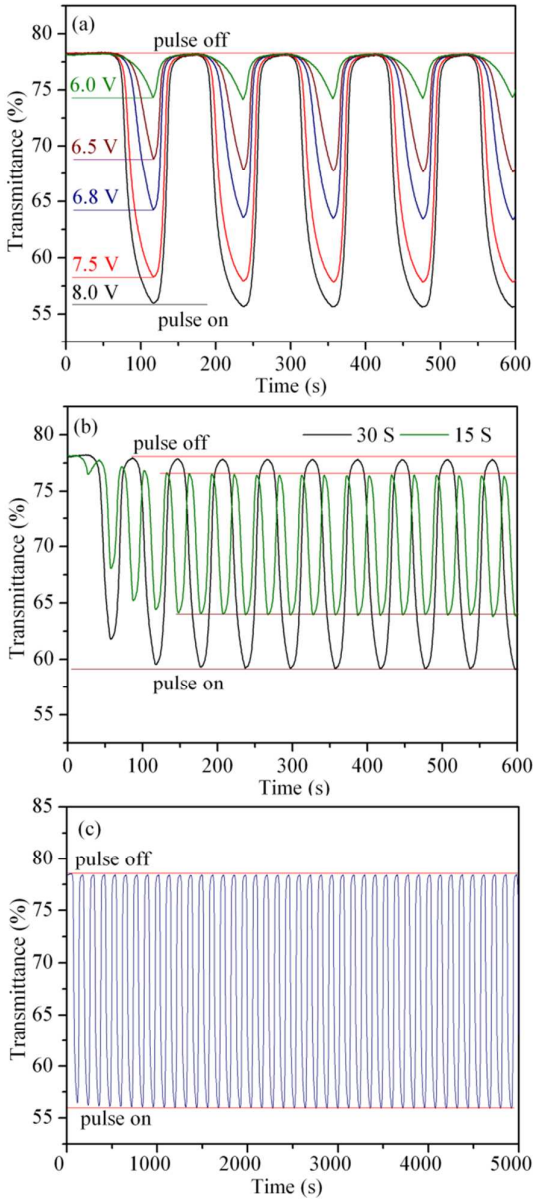

Fig. 6 Infrared transmittance of the device at 1.5 μm upon applied square-wave pulse with (a) different amplitudes, (b) different duration times and (c) amplitude of 8 V duration time of 1min.

duration time, the lower the equilibrium value because of a critical time is needed for the device to achieve a equilibrium temperature or recover to room temperature, as shown in Fig. 6b, in which when the duration time of a 8 V pulse changes from 30 to 15 s, the equilibrium infrared transmission changes from about 58 % to 64 %, and infrared transmission cannot recover its original value. Above results demonstrate that the infrared modulation can be tuned not only by the input pulse amplitude but also the duration time of the pulse. An optimal result in infrared modulation of the device at 1.5 μm upon an input 8 V square-wave pulse with 1 min duration time is shown in Fig. 6c. One can see that the infrared transmittance drops from about 78 % to 56 %, and about 22 % infrared modulation is realized. From Fig. 6c one also can see that after first two cycles the infrared

modulation is almost constant, demonstrating a high stability and reversibility of the device in response to an input pulse voltage.

In summary, the star-shaped VO_2 (D) nanoparticles were synthesized by a simple hydrothermal reaction in the presence of only ammonium metavanadate and formic acid, which can be transformed to VO_2 (M) NPs through a mild annealing treatment. The formic acid, hydrothermal temperature and pH value are important to obtain the star-shaped VO_2 (D) NPs. The absence of other reactants and surfactants can not only make it easier to handle the reaction but also avoid any organic residues in the resulted product, which is benefit for practical application as no superfluous wash is needed. The morphology and size of VO_2 (D) NPs nearly have no change after transforming to VO_2 (M) NPs. It was found that the lower the annealing temperature, the lower the phase transition temperature and the narrower the hysteresis width because of interface effect of the star-shaped VO_2 (M) NPs. The infrared modulation amplitude of the VO_2 (M) NPs thin films can be controlled by the thickness of the films, and the thicker the film the higher the infrared modulation amplitude. An excellent infrared modulation with high stability and reversibility has been demonstrated in the VO_2 (M) NPs/Ag NWs/glass device upon an applied pulse voltage, in which the infrared modulation amplitude can be controlled not only by the input pulse amplitude but also the duration time of the pulse. The VO_2 (M) NPs/Ag NWs/glass device might find potential applications in infrared electro-optical switch devices and infrared sensors.

Experimental

Materials synthesis: For a typical synthesis, 2 mmol ammonium metavanadate was dissolved in 20 ml deionized water with continue magnetic stirring for 30 min, then formic acid (88 wt%, 2 ml) was added drop by drop into the light yellow solution with magnetic stirring for 5~10 min. The precursor solution with a pH of about 2 was sealed in a 40 ml Teflon cup and placed in a sealed autoclave for hydrothermal treatment at 200 ^oC for 2 days in an oven. After cooling down to room temperature naturally, the precipitate was dried at 60 ^oC in air after cleaning by water and alcohol alternatively. The as-prepared powders were finally annealed at 300-450 ^oC for 1 h in a vacuum furnace (~20 Pa) to obtain VO_2 (M) NPs.

Characterization: The size, morphology and microstructure of the as-prepared and annealed powders were characterized by field-emission scanning electronic microscope (FESEM, Sirion 200), X-ray diffractometer with a Cu Kα line (XRD，Philips X'Pert) and transmission electronic microscope (TEM, JEOL Model 2010). The phase transition was analyzed by differential scanning calorimetry. (Netzsch DSC-204) with a heating and cooling rate of 10 ^oC/min in nitrogen atmosphere. The optical transmission spectra of the VO_2 (M) NPs thin films were recorded by UV-3600 spectrophotometer (Shimadzu ISR-260) and Fourier transform infrared (FTIR) spectrometer (Bruker Vector-22) equipped with temperature controller.

Acknowledgement

This work was financially supported by the National Natural Science Foundation of China (grant no. 51372250 and 51402304) and the Anhui province Natural Science Foundation (grant no. 1408085MKL54).

References

1. F. J. Morin, Phys Rev Lett, 1959, 3, 34.
2. J. Ni, W. Jiang, K. Yu, Y. Gao and Z. Zhu, Electrochimica Acta, 2011, 56, 2122-2126.
3. C. Wang, X. Liu, J. Shao, W. Xiong, W. Ma and Y. Zheng, RSC Advances, 2014, 4, 64021-64026.
4. P. Liu, K. Zhu, Y. Gao, Q. Wu, J. Liu, J. Qiu, Q. Gu and H. Zheng, CrystEngComm, 2013, 15, 2753.
5. D. Hagrman, J. Zubieta, C. J. Warren, L. M. Meyer, M. M. J. Treacy and R. C. Haushalter, J. Solid State Chem., 1998, 138, 178-182.
6. L. Liu, F. Cao, T. Yao, Y. Xu, M. Zhou, B. Qu, B. Pan, C. Wu, S. Wei and Y. Xie, New J. Chem., 2012, 36, 619.
7. E. Strelcov, Y. Lilach and A. Kolmakov, Nano Lett, 2009, 9, 2322-2326.
8. J. M. Baik, M. H. Kim, C. Larson, C. T. Yavuz, G. D. Stucky, A. M. Wodtke and M. Moskovits, Nano Lett, 2009, 9, 3980-3984.
9. G. Leahu, R. Li Voti, C. Sibilia and M. Bertolotti, Appl. Phys. Lett., 2013, 103, 231114.
10. A. Kar, N. Shukla, E. Freeman, H. Paik, H. Liu, R. Engel-Herbert, S. Bhardwaja, D. G. Schlom and S. Datta, Appl. Phys. Lett., 2013, 102, 072106.
11. J. C. Orlianges, J. Leroy, A. Crunteanu, R. Mayet, P. Carles and C. Champeaux, Appl. Phys. Lett., 2012, 101, 133102.
12. S. H. Bae, S. Lee, H. Koo, L. Lin, B. H. Jo, C. Park and Z. L. Wang, Adv. Mater., 2013, 25, 5098-5103.
13. Y. Gao, H. Luo, Z. Zhang, L. Kang, Z. Chen, J. Du, M. Kanehira and C. Cao, Nano Energy, 2012, 1, 221-246.
14. Y. Y. Luo, L. Q. Zhu, Y. X. Zhang, S. S. Pan, S. C. Xu, M. Liu and G. H. Li, J. Appl. Phys., 2013, 113, 183520.
15. C. Cheng, H. Guo, A. Amini, K. Liu, D. Fu, J. Zou and H. Song, Sci. Rep., 2014, 4, 5456.
16. C. Wu, X. Zhang, J. Dai, J. Yang, Z. Wu, S. Wei and Y. Xie, J. Mater. Chem., 2011, 21, 4509.
17. M. Li, S. L. Ji, J. Pan, H. Wu, L. Zhong, Q. Wang, F. D. Li and G. H. Li, J. Mater. Chem. A, 2014, 516, 3572-3576.
18. Z. Zhang, Y. Gao, L. Kang, J. Du and H. Luo, J. Phys. Chem. C, 2010, 114, 22214-22220.
19. S. A. Corr, M. Grossman, Y. F. Shi, K. R. Heier, G. D. Stucky and R. Seshadri, J. Mater. Chem., 2009, 19, 4362-4367.
20. Y. Z. Shidong Ji , Feng Zhang, Ping Jin, J. Crystal Growth, 2010, 312, 282-286.
21. D. Alie, L. Gedvilas, Z. Wang, R. Tenent, C. Engtrakul, Y. Yan, S. E. Shaheen, A. C. Dillon and C. Ban, J. Solid State Chem., 2014, 212, 237-241.
22. J. H. Son, J. Wei, D. Cobden, G. Cao and Y. Xia, Chem.Mater., 2010, 22, 3043-3050.
23. C. Cao, Y. Gao and H. Luo, J. Phys. Chem. C, 2008, 112, 18810-18814.
24. Luisa Whittaker, J. M. Velazquez and S. Banerjee, CrystEngComm, 2011, 13, 5328-5336.
25. B. Y. Qu, L. Liu, Y. Xie and B. C. Pan, Phys. Lett. A, 2011, 375, 3474-3477.
26. A. Pan, H. B. Wu, L. Yu and X. W. D. Lou, Angew. Chem. Int. Ed., 2013, 125, 2282-2286.
27. M. Li, X. Wu, L. Li, Y. Wang, D. Li, J. Pan, S. Li, L. Sun and G. Li, J. Mater. Chem. A, 2014, 2, 4520.
28. M. Li, D. B. Li, J. Pan, J. C. Lin and G. H. Li, Euro. J. Inorg.Chem., 2013, 2013, 1207-1212.
29. J. Liu, Q. Li, T. Wang, D. Yu and Y. Li, Angew. Chem. Int. Ed., 2004, 116, 5158-5162.
30. C. Cesari, C. Leroux and G. E. Nihoul, Key Eng. Mater., 1998, 155-156, 227-266.
31. I. M. Lifshitz and V. V. Slyozov, J. Phys. Chem. Solids, 1961, 19, 35-50.
32. R. L. Penn and J. F. Banfield, Geochim. Cosmochim. Ac, 1999, 63, 1549–1557.
33. Y. Li, S. Ji, Y. Gao, H. Luo, S. Li, M. Jiang, Y. Zhou, R. Li, B. Wang and P. Jin, CrystEngComm, 2013, 15, 8330-8336.
34. R. Lopez, L. Feldman and R. Haglund, Phys. Rev. Lett., 2004, 93,177403.
35. Y. Sun, S. Jiang, W. Bi, R. Long, X. Tan, C. Wu, S. Wei and Y. Xie, Nanoscale, 2011, 3, 4394-4401.
36. S. Wang, X. Zhang and W. Zhao, J. Nanomater., 2013, 2013, 1-6.
37. S. Ji, W. He, K. Wang, Y. Ran and C. Ye, Small, 2014, 10, 4951-4960.

Graphic Abstract

Star-shaped VO_2 (M) nanoparticles demonstrate adjustable phase transition temperature and excellent reversible infrared modulations in response to external voltage.